Towards approximate models of coulomb frictional moments in: I) revolute pin joints and II) spherical-socket ball joints

Ali Faraz and Shahram Payandeh

Experimental Robotics Laboratory (ERL)
School of Engineering Science
Simon Fraser University
8888 University Drive
Burnaby, British Columbia
Canada V5A 1S6
e-mail: shahram@cs.sfu.ca

Abstract: In general, the rigid-contact assumption has been used to estimate the frictional moment between two bodies in contact. In a multi-body connection, two types of passive interconnection are considered in this paper, namely pin joint and spherical-ball joint. The joints are assumed to be passive at the localized configuration space of the multi-body systems and are assumed to be actuated remotely. The traditional approach for modelling such frictional contact does not consider the elastic deformation of joints. Two approximate models are presented for both revolute pin joints and spherical-socket ball joints. The proposed models offer a more accurate estimation of the Coulomb frictional moment. The new models offer a compact solution which can be easily extended to other geometrical multi-body contact configuration with various degrees of clearance. The proposed models can be used in the dynamic modelling and control of multi-body systems in frictional contact.

Key words: Approximate frictional models, Pin joints, Spherical joints

1 Introduction

In general, all linkage mechanisms and multi-body systems consist of joints and linkages, and rotary joints are the most commonly used type of joints. Rotary joints consist of two general categories: a) revolute joints(providing one Degree of Freedom (DOF)), and b) spherical joints(up to three DOF). Specifically, the revolute pin joints and spherical socket-ball joints are used when the requirements include: a) relatively high radial loads at the joints, b) very high stiffness of the joints to reduce the vibrational tendencies of the system, and c) simple and compact joints design. However, these two types of joints have disadvantages(compared to low friction bearings with intermediate rolling elements) such as: a) lower operational speed, b) relatively shorter service life, and c) higher friction. This higher level of friction requires to estimate/predict the frictional moment caused by the joints

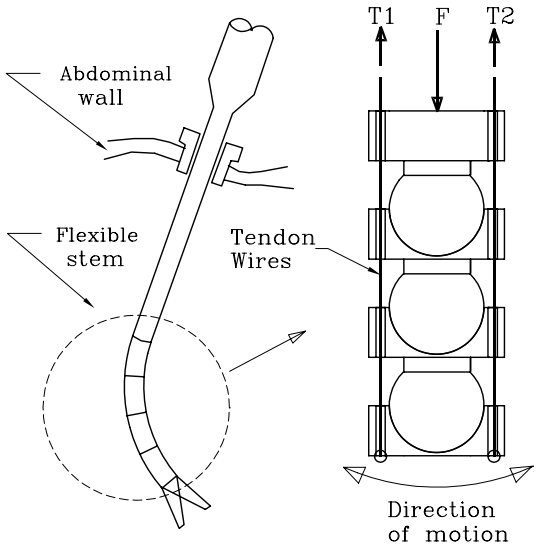

Figure 1: The flexible stem of an endoscopic tool.

more accurately both in static and dynamic cases. The motivation for accurate modeling of frictional moments in these types of joints are explained further by the following examples:

I) In the static cases(*e.g.* truss-cell systems[1], or endoscopic multi-jointed devices [2][3]), it is desired to predict/estimate the maximum frictional moment capacity of the static locked joints under different loading conditions.

II) In the dynamic cases of multi-body systems, the frictional moment at each joint is a contributing factor in the dynamic interaction between bodies. For accurate modeling of the system, it is essential to model frictional moment with the required accuracy[4] [5][6].

III) Another specific example (whit both static and dynamic applications) is the flexible stem in endoscopic tools which consist of several spherical joints (Figure 1). This allows the tools tip to have two degrees of freedom. Each joint is actuated by tendon like wires at the periphery. The unique feature of this design is that, these joints are held together, moved, and locked by changing the tension in the tendons. In the static case, when the joints are locked, the tension in the wires should exceed some minimum limit in order to prevent the joints from any slipping. However, in the dynamic case of moving joints, the tension must be reduced in some of the wires to allow the joints to rotate in the desired direction. In both of these cases it is important to estimate accurately the frictional moments of joints which are controlled by the tension of tendons.

As mentioned above, there are several papers related to experimental applications/studies of Coulomb frictional moment of joints [2] [6] [1], as well as general theoretical studies [4] [5]. Reference [7] is a good reference book on general modelling and solution to various contact mechanics problems. In all of these works, it is assumed that joints are absolutely rigid, and the contact is modeled as a point contact in the spherical socket-ball joints, and a line contact in revolute ones, where all the frictional force is concentrated on. This has led to simplified model for predicting the frictional moment.

However, in general there is a contact area caused by the elastic deformation of the joint that the Coulomb friction is acted on instead of the point contact. In this paper, contacts in the joints are considered elastic and using the elliptic load distribution over the contact surfaces, approximate models are developed which can predict/estimate the frictional moments with better accuracies. Finally, mathematical models for estimating the range of clearance in the joints, that ensures full contact and maximum stiffness of the pin and socket-ball joints, are presented.

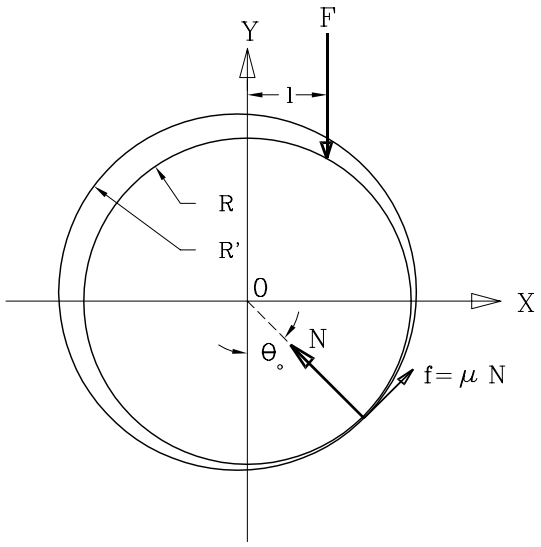

Figure 2: The rigid joint under load F.

2 Preliminary analysis

The simple derivation of current model is demonstrated here by the assumption of absolute rigidity of the joint with a point contact between its surfaces (Figure 2, the cross sectional view for both cases). The force F is the resultant external load acting on the joint (Figure 2), and the basic equilibrium of forces and moments for both cases are :

$\sum F_x = -N \sin\theta_0 + \mu N \cos\theta_0 = 0$

$\sum F_y = N \cos\theta_0 + \mu N \sin\theta_0 = F$

$\sum M_o = \mu N R = F l$

where

N = The reaction force at the contact point.

l = The distance of force F to the center of joint.

θ_0 = The equilibrium angle of contact point.

μ = The coefficient of friction between the two surfaces of joint.

The first equation leads to: $\tan\theta_0 = \mu$, and solving the other two equations, provides: $N = F/\sqrt{1+\mu^2}$, and :

$$\frac{l}{R} = \frac{\mu}{\sqrt{1+\mu^2}}. \tag{1}$$

Using the above equations, we can obtain the frictional moment acting on the joint ($M = \mu N R$) as:

$$M = F \times R \frac{\mu}{\sqrt{1+\mu^2}} \tag{2}$$

and for small values of μ (*e.g.* $\mu < 0{\cdot}3$), the value of $\sqrt{1+\mu^2}$ can be approximated to be equal to 1, Equations (1) and (2) reduce to: $l/R = \mu$, and $M = \mu F R$.

Equation 2 is used extensively in the literature [1]-[2] [4]-[6] to predict frictional moment in revolute or spherical joints. However, the above simplified analysis does not consider the elasticity of the joints. The following sections take into account the effects of elastic deformation and stress distribution over the contact area in revolute pin joints, and spherical socket-ball joints, in order to estimate the Coulomb frictional moment more realistically, and with higher accuracy.

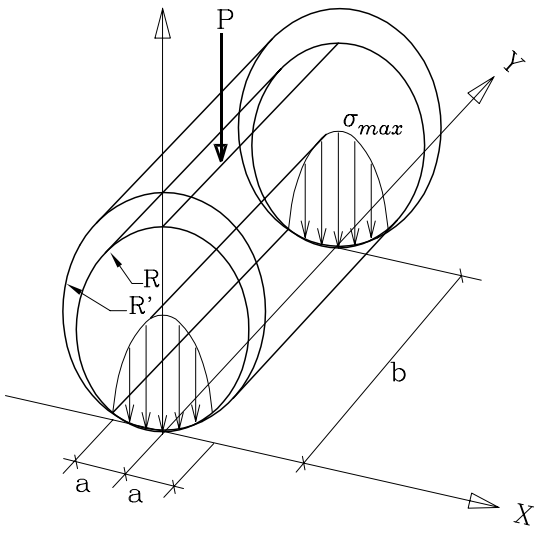

Figure 3: The stress distribution between two cylindrical surfaces.

3 Revolute pin joints

This section first presents the study of the stress distribution on the contact area of revolute joint, then by applying the Coulomb friction law at the contact area, the equilibrium analysis is carried out.

3.1 The radial stress distribution

The radial contact stress σ_r between the two cylindrical surfaces of radiuses R and R' due to deformation are known[8][10] to have elliptical distribution as:

$$\sigma_r = \sigma_{max}\sqrt{1 - \frac{x^2}{a^2}}. \tag{3}$$

When the material of the two surfaces are the same, with the module of elasticity E and Poisson ratio $\nu \approx 0{\cdot}3$ (true for most alloys), the maximum radial stress σ_{max} at the center line of contact region is :

$$\sigma_{max} = 0{\cdot}418\left[\frac{PE}{b}(\frac{R'-R}{RR'})\right]^{1/2} \tag{4}$$

and the width of contact area ($= 2a$, Figure 3) can be obtained by :

$$a = R\sin\alpha = 1{\cdot}25[\frac{P}{Eb}\frac{R'R}{R'-R}]^{1/2}, \tag{5}$$

where:

$b =$ The axial width of the revolute joint (Figure 3).

$P = F\cos\theta_0 =$ The radial component of load F.

$\alpha =$ Half of the maximum angular contact between the two cylinders (Figure 4).

When the material of the two surfaces are not the same, with different modules of elasticity of E_1, E_2, and Poisson ratios ν_1, ν_2, then E in the above equation is replaced by $1{\cdot}82E_1E_2/((1-\nu_2^2)E_1 + (1-\nu_1^2)E_2)$ [10].

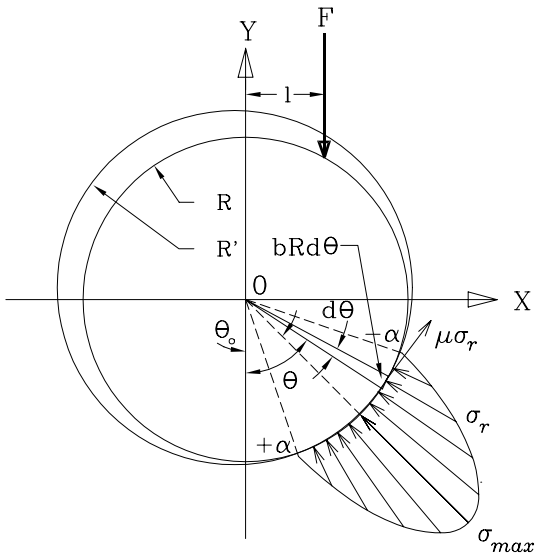

Figure 4: The revolute pin joint under load F.

We used Equation (3) for obtaining the radial stress distribution. It is assumed that the Coulomb frictional law can be used for obtaining the tangential stress distribution between two cylindrical surfaces of the joint.

3.2 Equilibrium analysis

Given the stress distributions on cylindrical surfaces, it is possible to write equilibrium equations of forces and moments. The components of forces acting on an infinitesimal area of contact $bR\mathrm{d}\theta$ (Figure 4) are:

$$\sum \mathbf{d\vec{F}} = \sigma_r bR\mathrm{d}\theta[(\mu\cos\theta - \sin\theta)\hat{\mathbf{i}} + (\cos\theta + \mu\sin\theta)\hat{\mathbf{j}}], \tag{6}$$

where $\sigma_r = \sigma_{max}\sqrt{1 - \frac{R^2}{a^2}\sin^2(\theta - \theta_0)}$ is obtained from Equation (3).

By integrating over the contact area, equilibrium equations of forces along x, y, and moment around z axis (Figure 4) could be written as:

$$\sum \mathbf{F}_x = \int_{\theta_0-\alpha}^{\theta_0+\alpha} \sum \mathbf{d\vec{F}} \cdot \hat{\mathbf{i}} = \int_{\theta_0-\alpha}^{\theta_0+\alpha} bR\sigma_{max}(\mu\cos\theta - \sin\theta)\sqrt{1 - \frac{R^2}{a^2}\sin^2(\theta - \theta_0)}\mathrm{d}\theta = 0, \tag{7}$$

$$\sum \mathbf{F}_y = \int_{\theta_0-\alpha}^{\theta_0+\alpha} \sum \mathbf{d\vec{F}} \cdot \hat{\mathbf{j}} = \int_{\theta_0-\alpha}^{\theta_0+\alpha} bR\sigma_{max}(\mu\sin\theta + \cos\theta)\sqrt{1 - \frac{R^2}{a^2}\sin^2(\theta - \theta_0)}\mathrm{d}\theta = F, \tag{8}$$

$$\sum \mathbf{M}_o = \int_{\theta_0-\alpha}^{\theta_0+\alpha} \left[\vec{\mathbf{R}} \times \sum \mathbf{d\vec{F}}\right] \cdot \hat{\mathbf{k}} = \int_{\theta_0-\alpha}^{\theta_0+\alpha} \mu bR^2\sigma_{max}\sqrt{1 - \frac{R^2}{a^2}\sin^2(\theta - \theta_0)}\mathrm{d}\theta = Fl, \tag{9}$$

where:

θ_0= the angle where maximum radial stress occurs (Figure 4).

$\vec{\mathbf{R}} = R(\sin\theta\hat{\mathbf{i}} - \cos\theta\hat{\mathbf{j}})$

l = the distance between force F and y axis (Figure 4).

By substituting for: $a = R\sin\alpha$, $u = \theta - \theta_0$, and the trigonometric expansion of Equations (7) and (8), can be solved and provide the following equations:

$$\tan\theta_0 = \mu, \tag{10}$$

$$F = \frac{\pi b.R}{2}\sigma_{max}(1+\mu^2)^{1/2}\sin\alpha. \tag{11}$$

On the other hand, equation (9) can not be solved analytically since it is an elliptic integral. There are various approaches of finding the solution for (9).

I) Numerical Integration: This method could be applied by using numerical integration algorithms to each individual case, however it is computationally intensive, and time consuming. This is true when the solution is needed for dynamic cases (such as the endoscopic flexible extenders), where load and other parameters are constantly changing.

II) Tabulated Values: There are tables for different kinds of elliptic integrals that could be used[9] to solve equation (9). Although not practical, they are used in this paper (Table 1) to verify the results of the next method (*Expansion Series*), and based on that, develop a convenient approximate solution.

III) Expansion Series: Approximation is possible by obtaining series expansion of the equation (9). For this purpose first let $K = R/a$ and $u = \theta - \theta_0$ to get equation (9) in the following form:

$$\frac{Fl}{\mu b R^2 \sigma_{max}} = \int_{-\alpha}^{\alpha} \sqrt{1 - K^2 \sin u^2}\mathrm{d}u = 2\mathcal{E}(\alpha, K), \tag{12}$$

where $\mathcal{E}(\alpha, K)$ is defined as *the normal elliptic integral of the second kind*[9], that could be represented with expansion series if $K < 1$. However in our case $K \geq 1$ since: $K = R/a$, and $a = R\sin\alpha$, so $K = 1/\sin\alpha$, since $1 \geq \sin\alpha \geq 0$ which results in: $K \geq 1$. Therefore, it is necessary to use *Reciprocal Modulus Transformation*[9] of $\mathcal{E}(\alpha, K)$ as :

$\mathcal{E}(\alpha, K) = [\mathcal{E}(\beta, k) - (1-k^2)\mathcal{F}(\beta, k)]/k$

Where $k = 1/K = \sin\alpha$, and $\beta = \sin^{-1}(K\sin\alpha) = \sin^{-1}(1) = \pi/2$. Also $\mathcal{F}(\beta, k)$ is *the normal elliptic integral of the first kind*. Then Equation (12) is transformed to:

$$\frac{Fl}{\mu b R^2 \sigma_{max}} = 2\mathcal{E}(\alpha, K) = 2[\mathcal{E}(\pi/2, k) - (1-k^2)\mathcal{F}(\pi/2, k)]/k. \tag{13}$$

Now by substituting (11) in (13), we can further reduce the expansion as:

$$\frac{l}{R} = \frac{4\mathcal{E}(\alpha, K)}{\pi\sin\alpha}\frac{\mu}{\sqrt{1+\mu^2}} = C_\alpha \frac{\mu}{\sqrt{1+\mu^2}}, \tag{14}$$

where

$$C_\alpha = \frac{4\mathcal{E}(\alpha, K)}{\pi\sin\alpha} = \frac{4}{\pi}[\mathcal{E}(\pi/2, k) - (1-k^2)\mathcal{F}(\pi/2, k)]/k^2. \tag{15}$$

The expansion series of $\mathcal{E}$, and $\mathcal{F}$[9] can be used to obtain an expansion series for C_α by applying them to Equation (15) as the followings:

$$\begin{aligned}
\mathcal{E}(\pi/2, k) &= \tfrac{\pi}{2}\left[1 - \tfrac{1}{4}k^2 - \tfrac{3}{64}k^4 - \tfrac{5}{256}k^6 - \tfrac{175}{16384}k^8 - .....\right], \\
\mathcal{F}(\pi/2, k) &= \tfrac{\pi}{2}\left[1 + \tfrac{1}{4}k^2 + \tfrac{9}{64}k^4 + \tfrac{25}{256}k^6 + \tfrac{1225}{16384}k^8 + ...\right], \\
C_\alpha &= 1 + \tfrac{1}{8}k^2 + \tfrac{3}{64}k^4 + \tfrac{25}{1024}k^6 + \tfrac{245}{16384}k^8 + ... \quad .
\end{aligned} \tag{16}$$

On the other hand, the tabulated values of $\mathcal{E}$ and $\mathcal{F}$[9] are used, and the following values of C_α based on equation (15) are calculated (Table 1) and plotted versus α in Figure 5 (shown by small circles).

α	$k = \sin\alpha$	$\mathcal{E}(\pi/2, k)$	$\mathcal{F}(\pi/2, k)$	$2\mathcal{E}(\alpha, K)$	C_α
0	0·0	1·57080	1·570796	0·0000	1·000
5	0·087	1·567809	1·573792	0·1370	1·001
15	0·259	1·544150	1·598142	0·4100	1·008
30	0·500	1·467462	1·685750	0·8126	1·035
45	0·707	1·350644	1·854075	1·1981	1·079
60	0·866	1·211056	2·156516	1·5517	1·141
75	0·966	1·076405	2·768063	1·8448	1·216
90	1·000	1·00000	∞	2·0000	1·273

Table 1: The values of C_α for different contact angles α .

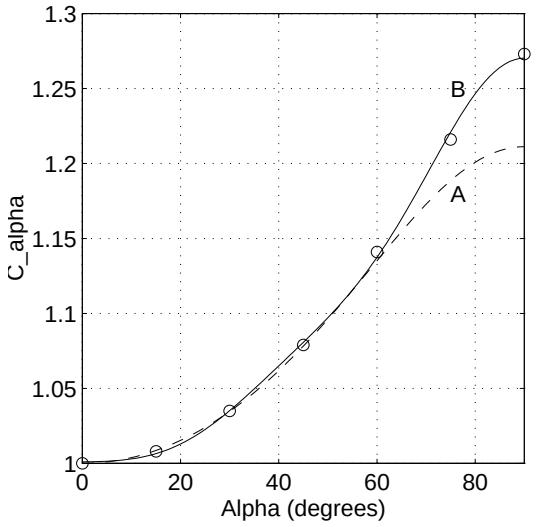

Figure 5: C_α *vs.* α for revolute pin joints.

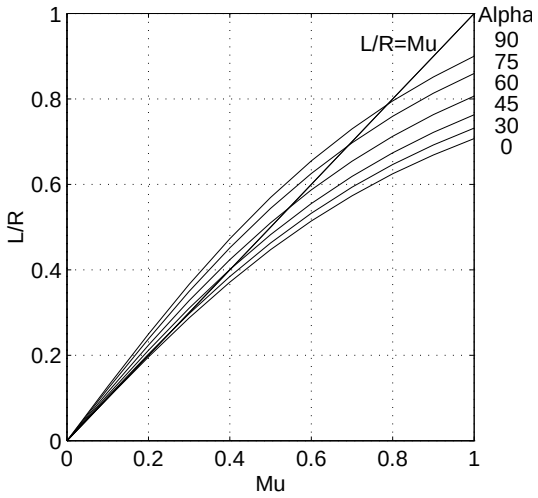

Figure 6: l/R *vs.* μ for revolute pin joints.

Comparing the results of these two approaches shows that, the series (16) converges to the final values of C_α (Table 1) very slowly as the number of elements in the series are increased. For example, even the summation of the first five elements of the series results in 5% deviation for large values of α (shown by the dashed line A, in Figure 5) from the tabulated values.

IV) Curve Fitting : By curve fitting techniques (to the data points of C_α from Table 1), it is possible to obtain functions with better accuracy compared to the results of expansion series with limited number of elements. For example, by knowing the type of polynomial obtained from previous section (*i.e.* equation 16), the function $C_\alpha = 1 + Ak^2 + Bk^4 + Ck6 + Dk^8$ could be solved by least square method for the tabulated values of C_α (from Table 1), to obtain the coefficients: A, B, C, and D. This results in:

$$C_\alpha = 1 + 0 \cdot 0477k^2 + 0 \cdot 5744k^4 - 1 \cdot 051k^6 + 0 \cdot 6982k^8. \tag{17}$$

The above equation has less than 1% deviation from the values of C_α over the whole range of α (shown by the solid line B, in Figure 5). This is a reasonable level of accuracy for most practical applications, but other optimal curve fitting techniques might even achieve higher accuracies.

Now by having the equation of C_α, the final frictional moment of the revolute pin joint can be written as :

$$M = F \times l = F \times R(1 + 0 \cdot 0477 \sin^2\alpha + 0 \cdot 5744 \sin^4\alpha - 1 \cdot 051 \sin^6\alpha + 0 \cdot 6982 \sin^8\alpha)\frac{\mu}{\sqrt{1+\mu^2}}, \tag{18}$$

where α can be obtained from (5) and (10) as:

$$\alpha = \sin^{-1}\left[(\frac{2 \cdot 31F}{Eb\sqrt{1+\mu^2}} . \frac{R'/R}{R'-R})^{1/2}\right].$$

From the above equation it is evident that the value of M for some specific force F depends only on the parameter l. So the ratio l/R $(= M/FR)$ can be considered as a dimension-less index that represents the maximum moment capacity of the joint, regardless of the revolute joints dimensions.

The quantity l/R from Equation (14) is plotted for different values of μ and α in Figure 6. In this plot, the curve corresponding to $\alpha = 0$ represents rigid joint model (since, for $\alpha = 0 : C_\alpha = 1$, and Equation (14) converts to Equation (1), and comparing it to the full contact case (where $\alpha = 90°$),

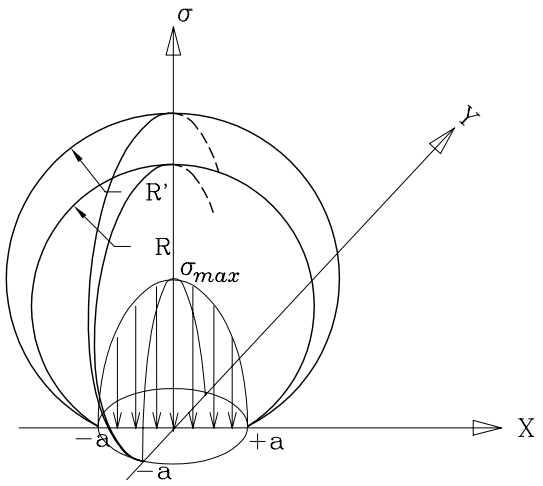

Figure 7: The stress distribution between two spherical surfaces.

Equation (1) has a deviation of 21% from Equation (18). This could result in the same amount of error, if equation (1) is used for a full contact case. Actually, the straight line approximation $l/R = \mu$ provides much better approximation for near full contact conditions than Equation (1). However, there is no need for approximation anymore, the new model (18) provides accurate estimation of M for any condition of friction and contact angle.

4 Spherical socket-ball joints

In this section, similar procedure as Section 3 is applied to spherical socket-ball joints. First, the stress distribution on the contact area of spherical joint is studied, then by applying Coulomb friction law at the contact area the equilibrium analysis is carried out.

4.1 The radial stress distribution

Similar to the cylindrical case (Equation 3), the radial contact stress σ_r between the two spherical surfaces of radiuses R and R' due to deformation are known[8][10] to be an elliptical distribution as well. However, the elliptic distribution is along two axis(*i.e.* X, and Y axis) :

$$\sigma_r = \sigma_{max}\sqrt{1 - \frac{x^2}{a^2} - \frac{y^2}{a^2}}. \tag{19}$$

When the material of the two surfaces are the same, with the module of elasticity E and Poisson ratio $\nu \approx 0{\cdot}3$ (true for most alloys), the maximum radial stress σ_{max} at the center of contact region is:

$$\sigma_{max} = 0{\cdot}389[PE^2(\frac{R - R'}{RR'})^2]^{1/3}, \tag{20}$$

and the radius of contact region ($= a$, Figure 7) can be obtained by :

$$a = R\sin\alpha = 1{\cdot}11[\frac{P}{E}\frac{RR'}{R - R'}]^{1/3}, \tag{21}$$

where:

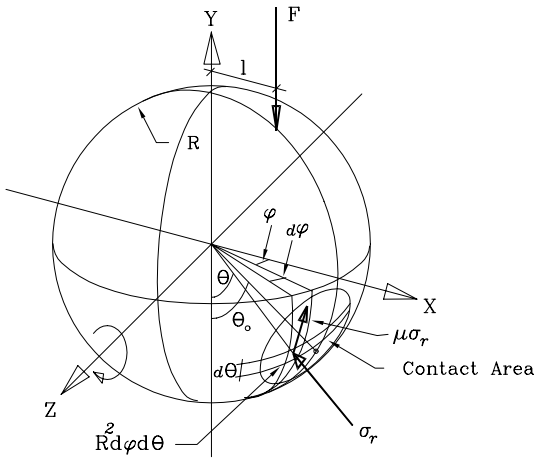

Figure 8: The spherical socket ball joint under load F.

$P = Fcos\theta_0 =$ The radial component of F.
$\alpha =$ Half of the maximum contact angle between the two spheres.

However, if the material of the two surfaces are not the same, then E in the above equation has to be changed with $1{\cdot}82E_1E_2/((1-\nu_2^2)E_1 + (1-\nu_1^2)E_2)$ as described in Section 3.1.

4.2 Equilibrium analysis

Based on the stress distribution on the spherical surface, the equilibrium equations of forces and moments can be obtained. First, by considering forces acting on an infinitesimal area, then integrating it over the whole contact area. The components of forces(normal and frictional tangent forces) acting on an infinitesimal area of contact $R^2\mathrm{d}\phi\ \mathrm{d}\theta$ (Figure 8) are:

$$\sum \mathbf{d\vec{F}} = \sigma_r R^2 \left[(-\cos\phi\sin\theta\hat{\mathbf{i}} + \cos\theta\cos\phi\hat{\mathbf{j}} - \sin\phi\hat{\mathbf{k}}) + \mu(\sin\theta\hat{\mathbf{j}} + \cos\theta\hat{\mathbf{i}})\right]\mathrm{d}\phi\mathrm{d}\theta. \tag{22}$$

By integrating over the contact area, equilibrium equations of forces along x, y, and moment around z axis (Figure 6) could be written as:

$$\sum \vec{\mathbf{F}}_x = \int_{\theta_0-\alpha}^{\theta_0+\alpha}\int_{-\alpha'}^{+\alpha'} \sum \mathbf{d\vec{F}}\cdot\hat{\mathbf{i}} = \int_{\theta_0-\alpha}^{\theta_0+\alpha}\int_{-\alpha'}^{+\alpha'} R^2\sigma_r(\mu\cos\theta - \cos\phi\sin\theta)\mathrm{d}\phi\mathrm{d}\theta = 0, \tag{23}$$

$$\sum \vec{\mathbf{F}}_y = \int_{\theta_0-\alpha}^{\theta_0+\alpha}\int_{-\alpha'}^{+\alpha'} \sum \mathbf{d\vec{F}}\cdot\hat{\mathbf{j}} = \int_{\theta_0-\alpha}^{\theta_0+\alpha}\int_{-\alpha'}^{+\alpha'} R^2\sigma_r(\cos\theta\cos\phi + \mu\sin\theta)\mathrm{d}\phi\mathrm{d}\theta = F, \tag{24}$$

$$\sum \vec{\mathbf{M}}_{\mathbf{z}} = \int_{\theta_0-\alpha}^{\theta_0+\alpha}\int_{-\alpha'}^{+\alpha'} \left[\vec{\mathbf{R}}\times\sum \mathbf{d\vec{F}}\right]\cdot\hat{\mathbf{k}} = \int_{\theta_0-\alpha}^{\theta_0+\alpha}\int_{-\alpha'}^{+\alpha'} \mu R^2\sigma_r\cos\phi\mathrm{d}\phi\mathrm{d}\theta = Fl, \tag{25}$$

where,

$\sigma_r = \sigma_{max}\sqrt{1 - [\frac{R}{a}\sin(\theta-\theta_0)]^2 - [\frac{R}{a}\sin\phi]^2}$,
$\vec{\mathbf{R}} = R(\cos\phi\sin\theta\hat{\mathbf{i}} - \cos\phi\cos\theta\hat{\mathbf{j}} + \sin\phi\hat{\mathbf{k}})$,
$l =$ the distance between force F and y axis (Figure 8),
$\theta_0 =$ The angular position of center of the contact area(Figure 8),
$\alpha' = \sin^{-1}\sqrt{\sin^2\alpha - \sin^2(\theta-\theta_0)}$.

After expansion of the Equations (23) and (24), they convert into elliptic integral forms which do not have analytical solutions. However, it is possible numerically to verify that the equation (23) leads to the same equation: $\tan\theta_0 = \mu$, for different values of μ and α. Now, by knowing

$\theta_0 = \tan^{-1}\mu$, it is possible to find the radial component of force F (*i.e.* $P = F\cos\theta_0$), which drives the two spherical surfaces into each other radially, and is the same as force P in Equations (20) and (21). As a result we can have:

$$P = F\cos\theta_0 = F/\sqrt{1+\mu^2}.$$

On the other hand, by multiplying Equation (20) by square of equation (21), we may obtain a relation between σ_{max} and P as :

$$\sigma_{max}(R\sin\alpha)^2 = 0{\cdot}388(1{\cdot}11)^2\left[P^3(\frac{E\Delta RR}{ER\Delta R})^2\right]^{1/3} = 0388(1{\cdot}11)^2P.$$

Replacing $P = F/\sqrt{1+\mu^2}$ in the above equation, a relationship between F, and σ_{max} can be obtained without solving Equation (24) as followings :

$$\sigma_{max} = \frac{0{\cdot}388(1{\cdot}11)^2}{R^2\sin^2\alpha\sqrt{1+\mu^2}}F. \tag{26}$$

Now by substituting σ_{max} given in (26) in the trigonometric form of Equation (19), we can write

$$\sigma_r = \sigma_{max}\sqrt{1-[\frac{R}{a}\sin(\theta-\theta_0)]^2-[\frac{R}{a}\sin\phi]^2} = \frac{0{\cdot}388(1{\cdot}11)^2}{R^2\sin^2\alpha\sqrt{1+\mu^2}}F\sqrt{1-[\frac{R}{a}\sin(\theta-\theta_0)]^2-[\frac{R}{a}\sin\phi]^2},$$

which provides us with σ_r, which can be used in equation (25). This makes it possible to integrate Equation (25), and obtain:

$$\pi\mu\frac{0{\cdot}388(1{\cdot}11)^2}{R^2\sin^2\alpha\sqrt{1+\mu^2}}FR^3\left[\cos\alpha-\alpha\frac{\cos 2\alpha}{\sin\alpha}\right] = Fl,$$

after simplification it leads to:

$$\frac{l}{R} = 0{\cdot}75\left[\frac{\cos\alpha}{\sin^2\alpha}-\alpha\frac{\cos 2\alpha}{\sin^3\alpha}\right]\frac{\mu}{\sqrt{1+\mu^2}}. \tag{27}$$

Equation (27) has the same basic structure as Equation (14) in the case of revolute pin joint(*i.e.* $l/R = C_\alpha\mu/\sqrt{1+\mu^2}$). However, C_α in this case is

$$C_\alpha = 0{\cdot}75\left[\frac{\cos\alpha}{\sin^2\alpha}-\alpha\frac{\cos 2\alpha}{\sin^3\alpha}\right]. \tag{28}$$

C_α is plotted versus α in Figure 9, which can be interpreted as the deviation of elastic joint (as a more realistic assumption), compared to the absolute rigid joint(as an ideal case assumption, where $C_\alpha = 1$).

Now, by use of Equation (28), the frictional moment of the spherical joint would be:

$$M = F\times l = \frac{3}{4}F\times R\left[\frac{\cos\alpha}{\sin^2\alpha}-\alpha\frac{\cos 2\alpha}{\sin^3\alpha}\right]\frac{\mu}{\sqrt{1+\mu^2}}, \tag{29}$$

where, α can be obtained from (21) as $\alpha = \sin^{-1}\left[(\frac{1{\cdot}367_F}{ER\Delta R\sqrt{1+\mu^2}})^{1/3}\right]$

Same as previous section, l/R is the dimensionless parameter that represents the frictional moment capacity (M), of the spherical socket ball joint regardless of its size. Hence, l/R of Equation (27) is plotted for different values of μ and α as shown in Figure 10. In this plot, the curve corresponding to $\alpha = 0$, represents the rigid joint model, and comparing to full contact case (where $\alpha = 90^\circ$), Equation (1) has a deviation of about 15%. This means, equation (1) would result 15% error, if used when the joint is in full contact.

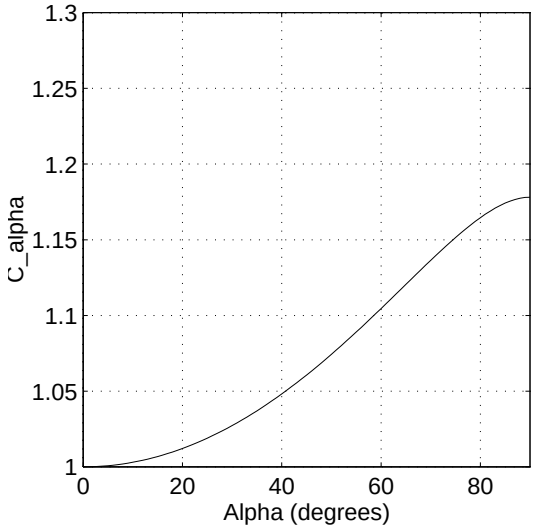

Figure 9: C_α vs. α for spherical socket ball joints.

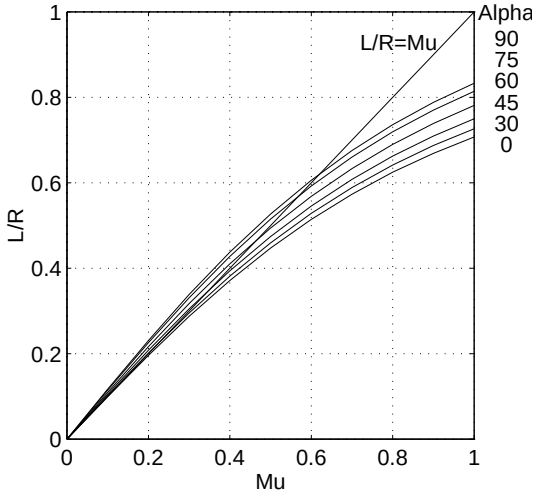

Figure 10: l/R vs. μ for spherical socket ball joints.

5 Discussions

Based on the previous analysis, we have presented the mathematical models (Equations (18), and (29)) that can predict the frictional moment M of the joints, as a function of the contact angle α, and μ. However, to apply these models effectively, it is important to know, under what range of loads on the joint, the value of α(and subsequently C_α, and M) is affected most. To clarify this in more details, the following questions must be addressed and discussed:

I) In what minimal range of loads, does the joint still behaves as a rigid joint(*i.e.* $\alpha \approx 0$, and $C_\alpha \approx 1$)?

II) In what intermediate range of loads, does the joint have partial contact as an elastic joint(*i.e.* $0 < \alpha < 90°$)?

III) In what maximal range of loads, does the joint have full contact as an elastic joint(*i.e.* $\alpha = 90°$)?

In order to answer the above questions, first we have to find the maximum load capacity of the joint P_{max}, as an upper bound limit, as well as a relative scale of comparison for other smaller loads(as the ratio P/P_{max}). The reason that P has been used here instead of the load force F is that, the radial load $P(= F\cos\theta_0)$ is the only contributing component of load F which is used in the computation of σ_{max}in Equations (4) and (20).

Let us first consider the revolute pin joints. Based on the strength of material(as the design criteria for maximum loading of joints), the maximum radial force P_{max} that can be exerted on the joint must not induce larger stresses than the allowable stress $\frac{\sigma_y}{S}$, where σ_y is the yield stress of the joint's material and S is the safety factor of design. Therefore σ_{max} in equation (4) can be replaced by $\frac{\sigma_y}{S}$ in order to find the maximum value of P defined as P_{max}. As a result :

$$P_{max} = \frac{5{\cdot}72b(R\sigma_y)^2}{E\Delta RS^2} \tag{30}$$

Where $\Delta R = R' - R$, and $R' \simeq R$ is assumed.

On the other hand, the full contact between the two cylindrical surfaces of the joint happens when the contact angle is $180°$(*i.e.* $\alpha = 90°$, Figure 4). Here, P_{fc} is defined as the minimum radial force required to cause *full contact* in the joint (*i.e.* $\alpha = 90°$). A relation for P_{fc} can be reached by substituting $\alpha = 90°$ in Equation (5):

$a = R\sin(90°) = 1{\cdot}52[\frac{P_{f.c.}}{Eb}\frac{RR'}{\Delta R}]^{1/2}$ And by assuming $R' \simeq R$, P_{fc} would be:

$$P_{fc} \geq \frac{Eb\Delta R}{2{\cdot}31}. \tag{31}$$

Now by dividing (31) by (30) and for revolute pin joints we can obtain the ratio of P_{fc} and P_{max} as :

$$1 \geq \frac{P_{fc}}{P_{max}} \geq 0{\cdot}076\left[S\frac{\Delta R}{R}\frac{E}{\sigma_y}\right]^2. \tag{32}$$

The same can be done for spherical socket-ball joints, that yields the following:

$$1 \geq \frac{P_{fc}}{P_{max}} \geq 0{\cdot}043\left[S\frac{\Delta R}{R}\frac{E}{\sigma_y}\right]^3. \tag{33}$$

As an example, let us look at a steel joint with normal design parameters such as: $\sigma_y = 500\text{MPa}, E = 210\text{GPa}, R = 10\text{mm}, \Delta R = 0{\cdot}01\text{mm}$, and the design safety factor of S=2·5 . Table 2

Type	Revolute Pin Joint			Spherical Socket-Ball Joint		
Contact	Low	partial	Full	Low	partial	Full
C_α	1·0 – 1·01	1·01 – 1·27	$1{\cdot}273 = \frac{4}{\pi}$	1·0 – 1·01	1·01 – 1·17	$1{\cdot}178 = \frac{3\pi}{8}$
α	0 – 20	21 – 89	90	0 – 18	19 – 89	90
$\frac{P}{P_{max}}$	0 – 0·01	0·01 – 0·08	0·08 – 1·0	0 – 0·001	0·001 – 0·05	0·05 – 1·0

Table 2: The typical calculated values of C_α, α, and $\frac{P}{P_{max}}$.

shows the typical calculated values for α, C_α, and P/P_{max} for the revolute and spherical cases. In this table, low contact refers to the narrow range of α that corresponds to the range of $1 \leq C_\alpha \leq 1{\cdot}01$. In other words, the low contact range represents the range of α(and the corresponding values of P/P_{max}), that $C_\alpha \simeq 1$, and the joint is still behaving rigid under the very light load. The partial contact is defined as the range that contact angle α is more than low contact range, but less than full contact(that $\alpha = 90^\circ$).

For revolute pin joints, from the above example it is apparent that, in order the assumption of rigid joint to be accurate ($C_\alpha \simeq 1$) then P should not exceed 1% (and 0·1%, in the case of spherical joint) of the maximum allowable load P_{max}.

On the other hand, in the full contact columns, when the load P exceeds 8% and 5% of P_{max}, then C_α is equal to 1·273, and 1·178 for revolute and spherical joints respectively. This is more than 90% of the range of allowable load P_{max}. Therefore assuming $C_\alpha = 1{\cdot}273$ (for revolute pin joints) and 1.178 (for spherical socket-ball) in the case of unknown loads(or when P is generally larger than $5 - 8\%$ of P_{max}), will result more accurate model than using the conventional model (2).

6 Concluding remarks

The elastic property of joints has led this study to the general formulation of the Coulomb frictional moment in the revolute pin joints or socket-ball joints as: $M = C_\alpha \frac{F \times R \times \mu}{\sqrt{1+\mu^2}}$

Where the value of C_α can generally be determined in the following three cases:

Case 1: For low contact angles(*e.g.* $\alpha \leq 20^\circ$), then $C_\alpha \simeq 1$. This corresponds to very light loads (*e.g.* about or less than 1% of joints allowable loads, Table 2), that the joints still acts as a rigid body.

Case 2: For partial contact(*e.g.* $20^\circ < \alpha \leq 90^\circ$) C_α can be calculated by the closed form Equations (17), and (28) for the two cases.

Case 3: For full contact (that $\alpha = 90^\circ$) C_α is equal to $1{\cdot}273(= 4/\pi)$, and $1{\cdot}178(= 3\pi/8)$ for the revolute and spherical joints, respectively.

Case 3 is the dominant case of joints operation (more than 90% of the designed load range), that could be used for general estimations when the exact magnitude of load P, or contact angle α are unknown, but the loads are high enough to cause full contact or near full contact(e.g. $\frac{P}{P_{max}} > 008$, Table 2).

In comparison to the conventional friction model(where $C_\alpha = 1$), the new model with the value of C_α obtained according to case 2 or 3 can prevent up to 21% and 15% error in the Coulomb frictional moment estimation of pin and socket-ball joints respectively. This higher accuracy is

specially important for better control, and dynamic modeling of multi-body systems with several joints in series(with accumulative error). One of such cases is the estimation of the frictional moments in the endoscopic flexible stems for locking and motion control of the extenders.

References

[1] H. S. Tzou and Y. Rong, Contact Dynamics of a Spherical Joint and a Jointed Truss-Cell System, *American Institute of Aeronautic and Astronautic Journal*, 29, 1991, 81–88

[2] R. H. Sturges and S. Laowattana, A Flexible, Tendon-Control Device for Endoscopy, *International Journal of Robotics research*,12, 1993, 121–131

[3] A. Faraz and S. Payandeh, Issues and Design Concepts in Endoscopic Extenders, Proceedings of 6th IFAC Symposium on Man/Machine Systems, pp. 109–114, 1995

[4] Y. J. Shin and C. H. Kim, An Analytical Solution for Spherical Joint Mechanism Including Coulomb Friction, *6th Inter. Pacific Conference on Automation Engineering*, 1991, 383–389

[5] L. J. Gutkowski and G. L. Kinzel, A Coulomb Friction Model for Spherical Joints, *ASME DE*, 45, 1992, 243–250

[6] I. Imam, M. Skrenier and J. P. Sadler, A New Solution to Coulomb Friction in Bearing Mechanism: Theory and Application, *Trans. ASME*, 103, 1981, 764–775

[7] K. L. Johnson, Contact Mechanics, *Cambridge University Press*, 1985, (Section 4.1, Chapter 7)

[8] R. G. Budyans, Advanced Strength and Applied Stress Analysis, *McGraw-Hill*, 1977, 151–160

[9] P. F. Byrd and M.D. Friedman, Handbook of Elliptic Integrals for Engineers and Scientists, *Springer-Verlag*, 1, 299–301

[10] C. Lipson and R. Juvinall, Handbook of Stress and Strength, *MacMillan*, 1963, 81–88